



Full Text View

[Volume 30, Issue 11 \(November 2000\)](#)

Journal of Physical Oceanography

Article: pp. 2788–2797 | [Abstract](#) | [PDF \(220K\)](#)

Branching Mechanism of the Tsushima Current in the Korea Strait

Yang-Ki Cho

Faculty of Earth Systems and Environmental Sciences and Institute of Marine Science, Chonnam National University, Kwangju, Korea

Kuh Kim

School of Earth and Environmental Sciences, Oceanography Program, Seoul National University, Seoul, Korea

(Manuscript received February 11, 1999, in final form December 17, 1999)

DOI: 10.1175/1520-0485(2000)030<2788:BMOTTC>2.0.CO;2

ABSTRACT

Hydrographic studies show the seasonal variation of the East Korean Warm Current (EKWC), which is a branch of the Tsushima Current along the Korean coast. To understand the dynamics of the branching mechanism of the TC in the Korea Strait, a hydraulic model with two active layers was investigated in a rectangular strait with varying depth. When the lower cold water flows southward in a shallow meridional channel from the deep northern basin, it separates from the eastern boundary because of the sloping bottom to conserve potential vorticity. After separation, the lower layer hugs the western boundary as the channel becomes shallow. In a region where the lower layer is absent due to separation, the northward flow in the upper layer has a positive relative vorticity to conserve potential vorticity because the bottom topography becomes deeper from south to north. The northward velocity has its maximum on the eastern boundary. This mechanism may explain the formation of the branch along the Japanese coast. The upper layer along the western boundary experiences shrinking of its water column because of the presence of the lower layer, and negative relative vorticities are induced to conserve potential vorticity. The negative relative vorticity intensifies the northward flow of the upper layer near the western boundary. This is believed to be the causal mechanism of the EKWC. If the top of the lower layer in the basin is deep, such as it is in winter, the lower layer cannot reach the strait since the Bernoulli potential of the lower layer is small. This may explain why the EKWC is absent in winter.

Table of Contents:

- [Introduction](#)
- [Branching of the Tsushima](#)
- [Two-layer hydraulic model](#)
- [Application to the Korea](#)
- [Summary and discussion](#)
- [REFERENCES](#)
- [FIGURES](#)

Options:


- [Create Reference](#)
- [Email this Article](#)
- [Add to MyArchive](#)
- [Search AMS Glossary](#)

Search CrossRef for:

- [Articles Citing This Article](#)

Search Google Scholar for:

- [Yang-Ki Cho](#)
- [Kuh Kim](#)

The Tsushima Current (TC), which determines the major hydrography in the “East Sea” (Sea of Japan), splits into two branches ([Sverdrup et al. 1942](#), p. 734; [Uda 1934](#)) in the Korea Strait ([Fig. 1](#) ). One branch flows along the Japanese coast and the other flows along the Korean coast; the latter is called the East Korean Warm Current (EKWC).



Numerical experiments of the circulation in the East Sea ([Yoon 1982](#); [Kawabe 1982](#)) explain the EKWC as a kind of permanent western boundary current that exists because of the planetary beta effect and explain the branch along the Japanese coast in terms of topographic effect.


However, [Kim and Legeckis \(1986\)](#) show that the EKWC is sometimes absent, and [Isoda and Saitoh \(1993\)](#) suggest that the formation of the EKWC is seasonal. [Cho and Kim \(1996\)](#) confirm the seasonality of the EKWC and suggest the possibility that the southward movement of Korea Strait bottom cold water (KSBCW) is responsible for the formation of the EKWC. Furthermore, [Cho and Kim \(1996\)](#) show that the change of potential vorticity due to the shrinking of the Tsushima warm water (TWW) along the Korean coast is greater than the planetary beta effect. [Isobe \(1994, 1997\)](#) also argues that the JEBAR effect in Korea Strait, which is caused mainly by cold water along the Korean coast in summer, supplies the negative vorticity. The absence of the EKWC bears an exceptional importance in terms of not only the branching mechanism but also the circulation in the East Sea.

The primary objective of this study is to understand the dynamics of the branching mechanism of the TC in the Korea Strait and to explain the seasonal variation of the EKWC. The Korea Strait deepens from south to north. The northern part is deeper than 150 m, except for the shallow coastal areas, whereas the southern part is shallower than 125 m except in a deep trough. The hydrography in the Korea Strait can be simplified as two layers: TC in the upper layer and KSBCW in the lower layer. A hydraulic model with two active layers in a rectangular strait will be investigated to understand the flow dynamics under conditions of varying channel depth.


Hydraulic problems in straits have received considerable attention ([Shen 1981](#); [Hogg 1983](#); [Pratt 1986](#); [Bormans and Garrett 1989a,b](#)) since [Gill \(1977\)](#) first generalized them. [Hogg \(1983\)](#) investigated a rotating hydraulic model of the two active layers in varying channel widths and applied it to the Vema Channel. He focused on the two layers that move in the same direction under a deep resting layer. Later, [Hogg \(1985\)](#) applied the same model to the Alboran Sea and Strait of Gibraltar where the upper two layers flow in opposite direction from one basin to the other. Our study is similar to Hogg's, but we examine a flow structure under the condition of varying bottom topography, whereas [Hogg \(1983, 1985\)](#) examined the effects of varying channel width.

2. Branching of the Tsushima Current

To investigate the physical characteristics in Korea Strait and the neighboring sea, and their temporal variation, surveys were conducted in April, June, August, and October 1991. Sixty CTD stations were taken at each time ([Fig. 2](#) ). Japanese CTD data (solid triangles in [Fig. 2](#) ) were used to cover the eastern part of the strait ([Yamaguchi Prefectural Open-Sea Fisheries Experimental Station 1992](#)). Routine hydrographic data taken by the Korean Fisheries Research and Development Agency at lines A, C, E, G, I, and J in February 1991 were also used.

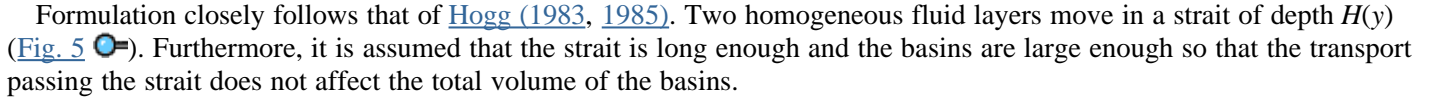
Analysis of the data by [Cho and Kim \(1998\)](#) shows that the KSBCW extends farther southward and becomes thicker in summer when the upper TWW becomes lighter. It retreats northward in winter when the TWW becomes denser. A temperature section taken along line D shows seasonal variation in the thickness of the KSBCW ([Fig. 3](#) ). In April, the section is occupied with warm water above 5°C except in two separate cores of cold water at the bottom of stations D1 and D3. In August the surface water warms up and a strong seasonal thermocline ($T = 16^{\circ}\sim 21^{\circ}\text{C}$) develops. At the same time, the KSBCW colder than 5°C appears extensively from stations D1 to D4. The coldest water of 2.8°C is found at the bottom of station D2.

Satellite images taken in 1991 and 1992 with concurrent hydrographic data showed branching of the TC in April and nonbranching in February ([Cho and Kim 1996](#)). Temperature distribution at the surface in February in 1989 and 1990 also showed the absence of the EKWC. Thus, branching was absent in February from 1989 to 1992, indicating that the absence of the EKWC is repeated in winter.

[Figure 4](#)  shows a schematic diagram for seasonal variation of the EKWC, depicting the horizontal and vertical distributions of cold water less than 5°C and the TWW warmer than 13°C in each season. The EKWC is formed when cold water appears in the strait and is absent when the cold water is present only at a deeper depth in the basin.

3. Two-layer hydraulic model in a rectangular channel with varying depth

a. Formulation

Formulation closely follows that of [Hogg \(1983, 1985\)](#). Two homogeneous fluid layers move in a strait of depth $H(y)$ ([Fig. 5](#) ). Furthermore, it is assumed that the strait is long enough and the basins are large enough so that the transport passing the strait does not affect the total volume of the basins.

The z axis is vertical, the y axis is along the strait, and the x axis is perpendicular to it. They form a right-handed Cartesian system. If the channel is long enough with respect to its width and variations in the y direction are sufficiently slow, then the alongstrait velocity component \mathbf{v} will be much greater than the cross-strait component u . The flow is assumed inviscid and in a steady state. See [Hogg \(1983, 1985\)](#) for details of mathematical formulations. The downstream balance can be expressed as

$$f\mathbf{v}_i = \frac{\partial(p_i/\rho_i)}{\partial x} \quad \text{and} \quad (1)$$

$$\mathbf{u}_i \cdot \nabla_h \mathbf{v}_i + fu_i = -\frac{\partial(p_i/\rho_i)}{\partial y}. \quad (2)$$

The subscript ($i = 1, 2$) denotes each layer, p pressure, ρ density, and $\mathbf{u} = (u, \mathbf{v})$ the horizontal velocity vector. Each layer satisfies a shallow water continuity equation:

$$\nabla_h \cdot \mathbf{u}_i D_i = 0. \quad (3)$$

The vertical force balance is assumed hydrostatic:

$$p_1 = -\rho_1 g(z_1 - \eta) \quad \text{and} \quad (4a)$$

$$p_2 = -g(\rho_2 - \rho_1)D_1 - \rho_2 g z_2 \\ + \rho_2 g(D_1 + D_2 - H), \quad (4b)$$

with

$$\eta = D_1 + D_2 - H.$$

A vorticity equation from [Eqs. \(1\)](#) and [\(2\)](#) can be expressed as

$$(\mathbf{u}_i \cdot \nabla_h) \left[\left(f + \frac{\partial \mathbf{v}_i}{\partial x} \right) D_i^{-1} \right] = 0.$$

For simplicity, the flow is assumed to have a uniform potential vorticity within each layer and f is constant.

Therefore

$$\left[\left(f + \frac{\partial \mathbf{v}_i}{\partial x} \right) D_i^{-1} \right] = \frac{f}{\hat{D}_i}, \quad (5)$$

where \hat{D}_i has an upstream potential depth equal to the actual layer thickness at points where the relative vorticity vanishes.

An equation for the Bernoulli potential B_i from [\(2\)](#) is

$$\left(f + \frac{\partial \mathbf{v}_i}{\partial x} \right) u_i = -\frac{\partial B_i}{\partial y} \quad (6)$$

with

$$B_i = \frac{p_i}{\rho_i} + \frac{1}{2} \mathbf{v}_i^2. \quad (7)$$

It is convenient to consider the above equations in a nondimensional form. Taking D_1^N (thickness of the upper layer at a northern upstream) for the depth scale, $a = (g'D_1^N)^{1/2}f^{-1}$ (the Rossby radius of deformation) for the length scale, af for a velocity scale, f^{-1} for a timescale, and $g'D_1^N$ for a pressure over density scale, the nondimensional equations become

$$\mathbf{v}_i = \frac{\partial p_i}{\partial x}, \quad (8)$$

$$\mathbf{u}_i \cdot \nabla_h \mathbf{v}_i + u_i = -\frac{\partial p_i}{\partial y}, \quad (9)$$

$$p_1 = -\hat{g}(H - D_1 - D_2), \quad \text{and} \quad (10a)$$

$$p_2 = -D_1 - \hat{g}(H - D_1 - D_2) \quad (10b)$$

with

$$\hat{g} = \frac{g}{g'} = \left(\frac{\rho_2}{\rho_2 - \rho_1} \right) \quad \text{and} \quad g' = g \left(\frac{\rho_2 - \rho_1}{\rho_2} \right)$$

describing the reduced gravity acting between two layers.

The nondimensional vorticity and Bernoulli equations are

$$1 + \frac{\partial v_i}{\partial x} = \frac{D_i}{\hat{D}_i} \quad \text{and} \quad (11)$$

$$\frac{D_i}{\hat{D}_i} u_i = -\frac{\partial B_i}{\partial y}, \quad (12)$$

where

$$B_i = p_i + \frac{\mathbf{v}_i^2}{2}. \quad (13)$$

We can obtain a coupled set of inhomogeneous second-order differential equations from (8), (10), and (11).

In the upper layer,

$$\frac{\partial^2 p_1}{\partial x^2} = \hat{g} \frac{\partial^2}{\partial x^2} (D_1 + D_2 - H) = \frac{D_1 - \hat{D}_1}{\hat{D}_1}. \quad (14a)$$

In the lower layer,

The Bernoulli constraint gives boundary conditions for the coupled second-order differential equations in the form

$$p_i + \frac{1}{2}v_i^2 = \pm \frac{Q_i}{2\hat{D}_i} + K_i \quad (15)$$

at

$$x = \pm \frac{1}{2}w.$$

Here Q_i is the total nondimensional transport in each layer. The constant K_i can be specified using the hydrostatic equation (10) and the conditions that $v_i = 0$ and $D_i = \hat{D}_i$ in the interior. See [Hogg \(1983\)](#) for details of boundary conditions.

The potential depth and the Bernoulli potential in the upstream of each layer are needed as input data for the model. We assume that the potential depths of the upper layer and the lower layer are \hat{D}_1 and \hat{D}_2 , respectively. Presence of a third layer in the northern basin does not affect the model result because it is not related directly to the potential depths and the Bernoulli potentials of the upper layers.

The boundary conditions involve the square of the layer velocity and are, therefore, nonlinear. Solutions are found using the packaged subroutine NLEQ from the International Mathematical Subroutine Library. The control depth and the separation depth (H_G) could be determined by this approach. Separation depth is a depth at which a layer separates from the boundary. Control depth is the minimum depth where long waves can no longer travel upstream at the control section when the fluid is accelerated to the section.

b. Results

There are a number of parameters to specify: channel width and depth, density ratios, potential depths, transports, and the division of the transport between upstream boundaries. The channel width is fixed and the control is achieved through varying the depth. We consider the parameters to represent flows in Korea Strait, which will be explained in detail in [section 4](#). Potential depths, density ratios, and transport parameters are taken as $\hat{D}_1 \equiv 1.2$, $\hat{D}_2 \equiv 1.5$, $\hat{g} = 604.176$, $Q_1 = 1.06$, $Q_2 = -0.053$, $\hat{\psi}_1 = -0.5Q_1$, $\hat{\psi}_2 = 0.5Q_2$.

Here $\hat{\psi}_i$ is the streamfunction in the upstream basin, which represents the relative current strength at the left boundary versus that at the right boundary. We assume that all transport of the upper moving layer is along the right (eastern) boundary in the upstream basin and transport for the lower layer is along the left (western) boundary.

The width of the lower layer is found as the depth decreases to a control section and then deepens again. In [Fig. 6](#) the lower layer width configurations for the specified upstream condition are shown as a function of the channel depth. When the depth is shallower than $H_s = 2.30$, the lower layer leaves the eastern boundary and the separation point is defined. The lower layer moves away from the eastern boundary if the depth decreases further. For depths shallower than 1.31 in nondimensional units, no solution is found. This is the control depth for which the slowest wave phase velocity vanishes. If the channel deepens again, the solution switches smoothly to another branch. Flow here is supercritical with respect to the slowest internal mode, and the lower layer accelerates quickly, similar to water flowing over a dam. These solutions, for the lower layer, look qualitatively similar to those given by [Gill \(1977\)](#) and [Whitehead et al. \(1974\)](#) for a one-layer problem: the lower layer is hydraulically controlled.

[Figure 7](#) shows the layer configurations and velocities before and after the control at the section whose depth is 1.50 in the strait. The lower layer shrinks along the western boundary and becomes thinner as the channel becomes shallow. This causes the negative relative vorticity to increase in the lower layer. The speed of the counterflow along the western boundary increases and the interface dips downward at the western boundary ([Fig. 7a](#)). Counterflow along the western boundary in the lower layer disappears, if the depth becomes shallow to the control section ($H = 1.31$) (not shown here). After the hydraulic control, the thickness and the width of the lower layer decrease in spite of the depth increase, as shown in [Fig. 6](#). [Figure 7b](#) shows layer configuration and velocity after the control at the section whose depth is 1.50.

Increase of the water depth and separation of the lower layer from the eastern boundary stretches the upper layer in the eastern part. This causes an increase in positive vorticity and velocity along the eastern boundary to conserve potential vorticity. On the western boundary, however, the thickness of the upper layer decreases due to the presence of the lower layer. This makes the negative vorticity and the velocity increase (Fig. 7a). After the control, the lower layer is too thin to make the negative vorticity of the upper layer increase (Fig. 7b). Northward flow in the upper layer appears only in the eastern part of the strait.

We calculate the velocity structure of the upper layer as the upper-layer thickness (D_1^N) in the northern basin changes. When the upper layer (D_1^N) in the northern upstream is thinner by 0.2 than that for Fig. 7, that is, if the Bernoulli potential of the lower layer in the upstream increases, then the lower layer becomes thicker and wider in the strait before the control point (Fig. 8). The thick lower layer causes an increase in both negative relative vorticity of the upper layer and northward speed along the western boundary. The high speed of the upper layer makes the interface near the western boundary rise to adjust the geostrophic balance between the two layers. The layer configuration and velocity structure after the control show little change, as in Fig. 7b (not shown here).

If the upper layer in the northern upstream is thicker by 0.2, then the lower layer becomes thinner and narrower in the strait. The thin lower layer causes a decrease in both the negative relative vorticity of the upper layer and northward speed of the upper layer along the western boundary. Low speed makes the interface near the western boundary dip downward (Fig. 9). The structure of the lower layer after the control is similar to the previous case (not shown here).

The velocity along the western boundary (V_w), the velocity along the eastern boundary (V_e), and the maximum southward velocity in the central region of the strait (V_m) are calculated to examine the variability of the upper-layer flow at the section whose depth is 1.50, as the thickness of the upper layer in the northern basin (D_1^N) changes. The V_w changes greatly from 0.95 to -0.05 as D_1^N changes from 0.65 to 1.20 (Fig. 10), whereas the V_m and the V_e change little. The lower layer in the strait becomes thinner as D_1^N increases, which results in the decrease of the V_w . A thick D_1^N makes the flow along the western boundary of the upper layer in the strait weaker, whereas a thin D_1^N makes it stronger.

4. Application to the Korea Strait

The East Sea can be divided into three layers (Moriyasu 1972): the upper TWW, the middle salinity minimum layer (SML) water (the North Korean cold water or/and the East Sea/intermediate water), and the lower East Sea proper water (ESPW). Because the KSBCW originates from the SML water (Kim and Kim 1983; Kim et al. 1991; Cho and Kim 1998), we assume that the ESPW is at rest. Thus the East Sea can be simplified as two moving layers: the upper warm layer above the permanent thermocline and the lower SML. The Korea Strait can also be simplified as two moving layers with the TWW and the KSBCW.

The SML water, characterized with $1^\circ \sim 5^\circ\text{C}$, is mainly located from 100 to 250 m in the Ulleung Basin (Cho and Kim 1998). Therefore, we can assume that the thickness of the upper and the lower layers in the northern basin (D_1^N and \hat{D}_2 in the model) are approximately 100 and 150 m, respectively. These values were used in the model.

The model section might represent section D in the station map (Fig. 11). It has a relatively flat bottom at approximately 150 m, except for the shallow region near the coast. The southern part is shallower than 125 m, except in a deep trough. The topography near the Korean coast in the southern part is not flat. The sloping effect of the bottom topography could affect the structure of the lower layer in the sloping region as Park et al. (1995) suggested.

When the lower layer flows into the shallow channel, it leaves the eastern boundary due to the potential vorticity constraint. The separation depth calculated by the model is about 230 m. After separation, the lower layer hugs the western boundary as the channel becomes shallow. This may explain why the KSBCW is observed only close to the Korean coast, irrespective of water depth.

In most hydraulic problems, hydraulic control occurs at a minimum section (Gill 1977; Whitehead et al. 1974). After the control, the counterflow vanishes and the width of the lower layer becomes smaller by far than that before the control, and it decreases as the channel depth increases. Korea Strait, however, becomes continuously shallower from the northern basin to the study section (section D in Fig. 11) except in the coastal region. Moreover, the calculated width of the lower layer (6 km) after the control is too small compared with those observed (30~50 km) in section D, whereas the width of the lower layer before the control (40 km) is comparable. Therefore, the hydraulic control is unlikely upstream of the study

section. It is possible, however, that a hydraulic control occurs in the downstream of section D, as [Park et al. \(1995\)](#) suggested, because there is a shallow region along the Korean coast ([Fig. 11](#)). But the hydraulic control downstream does not affect the layer configuration and velocity in the study section.

The northward TC in the Korea Strait has a positive relative vorticity, based on the vertical stretch caused by the increase of the water depth from 120 to 150 m. Therefore, the northward velocity near the Japanese coast increases, and this is considered as the formative mechanism of the first branch of the TC. Along the Korean coast, however, the TC meets the bottom cold water, shrinks, and has negative relative vorticity. The thickness of the upper layer near the Korean coast is about 100 m at section D in August, which is comparable with the model result. This change of relative vorticity due to shrinking of the upper layer from 120 to 100 m may intensify the northward flow of the TC near the Korean coast.

The positive relative vorticity along the eastern boundary and the negative relative vorticity along the western boundary produce the southward flow in the central region of the strait. This may explain the occurrence of the southward currents in the central region of Korea Strait ([Miita and Ogawa 1984](#); [Katoh 1994](#)). [Figure 12](#) shows the velocity section by direct observation across Korea Strait ([Miita and Ogawa 1984](#)) in summer. The section was taken as a line about 20 km south from the D line. Its depth is similar to that of the D line. It shows two northward flows along the coast and a southward flow in the central region of the strait.

The observed current is stronger along the west coast than that along the east coast, whereas current calculated by the model along line D is weaker along the west coast, as shown in [Fig. 7](#). This discrepancy could be explained by two reasons: 1) the narrow west channel of Korea Strait could accelerate the flow along the Korean coast in actual flow and 2) the relative velocity along the west coast can exceed that along the east coast when the thickness of the upper layer in the northern basin is thinner than the value used in the model, as shown in [Fig. 10](#).

We previously reported that the location of the SML in the Ulleung Basin changes vertically with season ([Cho and Kim 1998](#)). [Cho and Kim \(1998\)](#) suggested that it could be related to the density of the upper layer, because they observed that the cold water moves farther south in summer when the density of the upper layer decreases in Korea Strait. [Figure 13](#) shows the 5°C isotherms, which represent the upper boundary of the SML in section E for each month. The depth of the isotherm changes from 100 to 200 m. It is shallowest in August and deepest in February. The isotherm in February at depth 140~200 m is deeper by about 20~40 m than those in other months. It is certain that the depth of the SML in the Ulleung Basin becomes deeper in winter.

Our model shows that the presence of the flow along the west coast is affected by the thickness of the upper layer in the upstream basin (D_1^N). When the top of the SML is deep (i.e., large D_1^N) as in February, the volume of the KSBCW decreases in the strait. This makes the velocity of the upper layer along the western coast weaker, as shown in [Fig. 9](#). In that case, most northward flow in the upper layer exists along the eastern boundary. This is consistent with hydrographic observations, which show no branching in February when the bottom cold water is thinnest.

5. Summary and discussion

Recent hydrographic studies show the absence of the EKWC in winter. A two-layer rotating hydraulic model is applied to explain dynamically the seasonal variation of the EKWC. When the lower layer flows southward in a shallow meridional channel from the deep northern basin, it separates from the eastern boundary because of the sloping bottom in order to conserve potential vorticity. After separation, the lower layer hugs the western boundary as the channel becomes more shallow.

In a region where the lower layer is absent, the northward flow in the upper layer has a positive relative vorticity to conserve potential vorticity because the bottom becomes deeper from south to north. Therefore, the northward velocity has its maximum on the eastern boundary. This may explain the formation mechanism of the branch along the Japanese coast. However, the upper layer along the western boundary experiences shrinking of its water column because of the presence of the lower layer, generating negative relative vorticities to conserve potential vorticity. The negative relative vorticity intensifies the northward flow of the upper layer near the western boundary. This mechanism explains the other branch along the Korean coast, which has been known as the EKWC.

A beta effect may play a role in the formation of the EKWC, however; [Cho and Kim \(1996\)](#) showed that the change of relative vorticity due to the shrinkage of the water column in this area is greater by one order of magnitude than that due to the planetary beta effect.

When the SML layer in the basin is deep (i.e., small Bernoulli potential) as in winter, the volume of the KSBCW in the strait decreases due to the smaller potential energy. With smaller Bernoulli potential of the lower layer, the model suggests that the lower layer could not shrink the upper layer along the western boundary. Thus, the negative relative vorticity is not induced in the upper layer. This may explain the absence of the EKWC in winter. The wind effect could be another factor

for the absence of the EKWC in real flow in winter. The northerly wind in this area might prevent the formation of the northward EKWC because it is stronger than 1 dyn cm^{-2} in winter (Na et al. 1992).

The positive relative vorticity on the eastern side and the negative relative vorticity on the western side may induce the southward flow in the central region of the strait.

There are several defects in the present model. The velocity of the lower layer obtained from model seems too high when compared to the 20 cm^{-1} measured directly by [Isobe et al. \(1991\)](#). We do not know the transport upstream and do not consider the frictional effect, which may reduce the speed and alter the structure of the lower layer. [Smith \(1975\)](#) showed that the flow affected by friction may cross the isobath. Many observations ([Lim and Chang 1969](#); [Cho and Kim 1998](#)) show the KSBCW in a deep trough, rather than on the western side in the western channel of the Korea Strait. We regard these as secondary phenomena that might be elaborated in refinements to our model.

Acknowledgments

This research was supported in part by the Basic Sciences Research Institute Program, Korea Ministry of Education, 1998; the Korean Science and Engineering Foundation also supported this research, 1996–98. One of the authors (K. Kim) was supported by the Lotte Foundation in 1998–99 and Ocean Lab. in 1999–2000.

REFERENCES

- Bormans, M., and C. Garrett, 1989a: The effect of rotation on the surface inflow through the Strait of Gibraltar. *J. Phys. Oceanogr.*, **19**, 1535–1542. [Find this article online](#)
- , and —, 1989b: The effects of nonrectangular cross section, friction, and barotropic fluctuations on the exchange through the Strait of Gibraltar. *J. Phys. Oceanogr.*, **19**, 1543–1557. [Find this article online](#)
- Cho, Y.-K., and K. Kim, 1996: Seasonal variation of the East Korea Warm Current and its relation with the cold water. *La Mer*, **34**, 172–182.
- , and —, 1998: Structure of the Korea Strait Bottom Cold Water and its seasonal variation in 1991. *Contin. Shelf Res.*, **18**, 791–804.
- Gill, A. E., 1977: The hydraulics of rotating-channel flow. *J. Fluid Mech.*, **80**, 641–671.
- Hogg, N. G., 1983: Hydraulic control and flow separation in a multi-layered fluid with applications to the Vema Channel. *J. Phys. Oceanogr.*, **13**, 695–708. [Find this article online](#)
- , 1985: Multilayer hydraulic control with application to the Alboran Sea circulation. *J. Phys. Oceanogr.*, **15**, 454–466. [Find this article online](#)
- Isobe, A., 1994: Seasonal variation of the vertically averaged flow caused by the JEBAR effect in Tsushima Strait. *J. Oceanogr.*, **50**, 617–633.
- , 1997: The determinant of the volume transport distribution of the Tsushima Warm Current around the Tsushima/Korea Straits. *Contin. Shelf Res.*, **17**, 319–336.
- , A. Kaneko, S.-K. Byun, S. D. Chang, and S. Tawara, 1991: On the current structures in the western channel of the Tsushima/Korea Strait—From the result of the ADCP surveys in September 1989. *Eng. Sci. Rep. Kyushu Univ.*, **13**, 45–51.
- Isoda, Y., and S. Saitoh, 1993: The northward intruding eddy along the east coast of Korea. *J. Oceanogr.*, **49**, 443–458.
- Katoh, O., 1994: Structure of the Tsushima Current in the southwestern Japan Sea. *J. Oceanogr.*, **50**, 317–338.
- Kawabe, M., 1982: Branching of the Tsushima Current in the Japan Sea, Part 2. Numerical experiment. *J. Oceanogr. Soc. Japan*, **38**, 183–192.
- Kim, C. H., and K. Kim, 1983: Characteristics and origin of the cold water mass along the east coast of Korea (in Korean with English abstract). *J. Oceanol. Soc. Korea*, **18**, 73–83.
- Kim, K., and R. Legeckis, 1986: Branching of the Tsushima Current in 1981–83. *Progress in Oceanography*, Vol. 17. Pergamon, 256–276.
- , K.-R. Kim, J.-Y. Chung, and H.-S. You, 1991: Characteristics of physical properties in the Ulleung Basin. *J. Oceanol. Soc. Korea*,

Lim, D. B., and S. Chang, 1969: On the cold water mass in the Korea Strait. *J. Oceanol. Soc. Korea*, **4**, 71–82.

Miita, T., and Y. Ogawa, 1984: Tsushima currents measured with current meters and drifters. *Ocean Hydrodynamics of the Japan and East China Seas*, T. Ichiye, Ed., Elsevier Sciences, 67–76.

Moriyasu, S., 1972: The Tsushima Current. *The Kuroshio, its Physical Aspects*, H. Stommel and K. Yoshida Eds., University of Tokyo Press, 353–369.

Na, J., J. W. Seo, and S. K. Han, 1992: Monthly-mean sea surface winds over the adjacent seas of the Korean Peninsula. *J. Oceanol. Soc. Korea*, **27**, 1–10.

Park, Y.-G., Y.-K. Cho, and K. Kim, 1995: A hydraulic model of the Korea Strait Bottom Cold Current. *J. Oceanogr.*, **51**, 713–727.

Pratt, L. J., 1986: Hydraulic control of sill flow with bottom friction. *J. Phys. Oceanogr.*, **16**, 1970–1980. [Find this article online](#)

Shen, C. Y., 1981: The rotating hydraulics of the open-channel flow between two basins. *J. Fluid Mech.*, **112**, 161–188.

Smith, P. C., 1975: A streamtube model for bottom boundary current in the ocean. *Deep-Sea Res.*, **22**, 853–873.

Sverdrup, H. U., M. W. Johnson, and R. J. Fleming, 1942: *The Oceans, Their Physics, Chemistry and General Biology*. Prentice-Hall, 1087 pp.

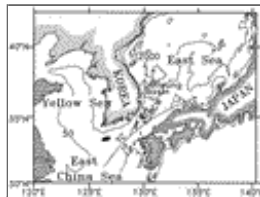
Uda, M., 1934: Results of simultaneous oceanographic investigations in the Japan Sea and its adjacent waters during May and June, 1932. *J. Imp. Fish. Exp. Stn.*, **5**, 57–190.

Whitehead, J. A., A. Leetmaa, and R. A. Knox, 1974: Rotating hydraulics of strait and sill flows. *Geophys. Fluid Dyn.*, **6**, 101–125.

Yamaguchi Prefectural Open-Sea Fisheries Experimental Station, 1992: Reports on affairs for forecasting fishery and oceanographic conditions in the 1991 fiscal years (in Japanese). 76 pp. [Available from Yamaguchi Prefectural Open-Sea Fisheries Experimental Station, Japan.]

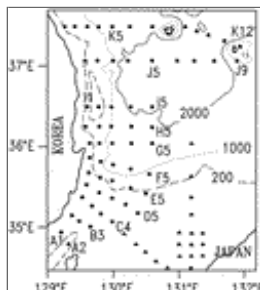
Yoon, J. H., 1982: Numerical experiment on the circulation in the Japan Sea, Part I: Formation of the East Korean Warm Current. *J. Oceanogr. Soc. Japan*, **38**, 43–51.

Figures



[Click on thumbnail for full-sized image.](#)

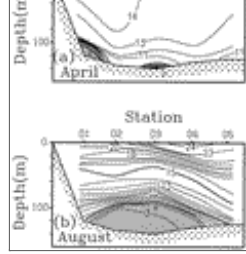
Fig. 1. Bathymetry and schematic circulation pattern of the Korea Strait and neighboring sea. TC and KSBCW denote the Tsushima Current and the Korea Strait bottom cold water. Study area is marked by a rectangular box. Depths are in meters



[Click on thumbnail for full-sized image.](#)

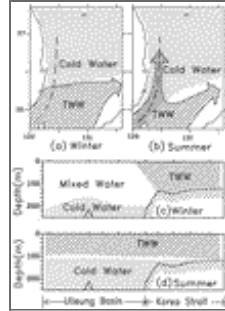
Fig. 2. CTD stations taken in Apr, Jun, Aug, Oct 1991. Numbers represent depth. Solid triangles represent Japanese stations





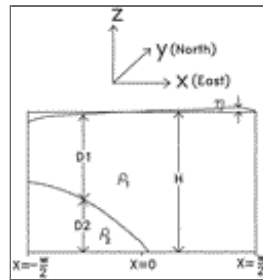
[Click on thumbnail for full-sized image.](#)

Fig. 3. Vertical sections of temperature along line D in (a) Apr and (b) Aug 1991



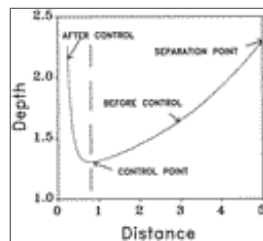
[Click on thumbnail for full-sized image.](#)

Fig. 4. Schematic distribution of the lower cold water (shadow area) and the upper TWW (hatched area) in winter (a, c) and summer (b, d). (a) and (b) are horizontal distributions, and (c) and (d) are vertical sections along the dashed lines in (a) and (b)



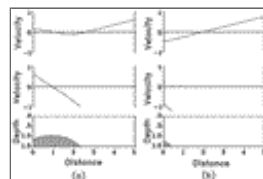
[Click on thumbnail for full-sized image.](#)

Fig. 5. Model section with two moving layers



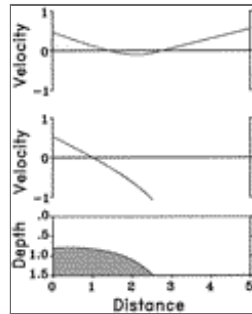
[Click on thumbnail for full-sized image.](#)

Fig. 6. The width of the lower layer with depth calculated from model ($\hat{D}_1 = 1.2$, $D_1^N = 1.0$, $\hat{D}_2 = 1.5$, $Q_1 = 1.06$, $Q_2 = 0.053$, $\psi_1 = -0.5Q_1$, $\psi_2 = 0.5Q_2$, $W = 5.0$). The separation depth (H_s) and the control depth (H_c) are 2.30 and 1.31, respectively



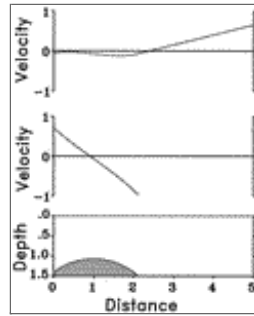
[Click on thumbnail for full-sized image.](#)

Fig. 7. Layer configuration and velocity when the depth (H) is 1.5; other parameters as in [Fig. 6](#). (a) Before the control and (b) after the control



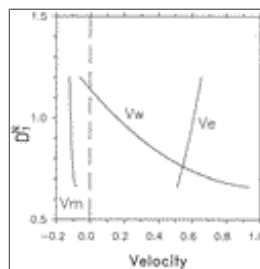
Click on thumbnail for full-sized image.

Fig. 8. As in Fig. 7a except for $D_1^N = 0.8$



Click on thumbnail for full-sized image.

Fig. 9. As in Fig. 7a except for $D_1^N = 1.2$



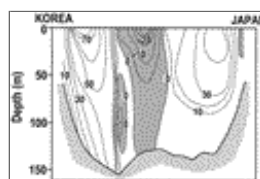
Click on thumbnail for full-sized image.

Fig. 10. The velocity of the upper layer with the thickness of the upper layer in the northern basin (D_1^N); V_e and V_w represent the velocities along the eastern and the western boundary, respectively, and V_m is the minimum velocity in the central region of the strait



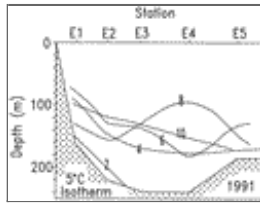
Click on thumbnail for full-sized image.

Fig. 11. Bottom topography of the Korea Strait. Depths are in meters



Click on thumbnail for full-sized image.

Fig. 12. Section of velocity by direct observation across Korea Strait from Miita and Ogawa (1984). Numbers are velocities in centimeters per second. Southward flow region is hatched



Click on thumbnail for full-sized image.

Fig. 13. The 5°C isotherms of section E at each month in 1991. Numbers indicate months of observation

Corresponding author address: Dr. Yang-Ki Cho, Faculty of Earth Systems and Environmental Science, Chonnam National University, 500-757 Kwangju, Korea.

E-mail: ykcho@chonnam.chonnam.ac.kr

top ▲



© 2008 American Meteorological Society [Privacy Policy and Disclaimer](#)
Headquarters: 45 Beacon Street Boston, MA 02108-3693
DC Office: 1120 G Street, NW, Suite 800 Washington DC, 20005-3826
amsinfo@ametsoc.org Phone: 617-227-2425 Fax: 617-742-8718
[Allen Press, Inc.](#) assists in the online publication of AMS journals.